Fluid Flow in An Evaporating Droplet

H. Hu and R. Larson, Department of Chem. Eng., University of Michigan,
2300 Hayward St., Ann Arbor, MI 48109.

ABSTRACT

Droplet evaporation is a common phenomenon in everyday life. For example, when a droplet of coffee or salt solution is dropped onto a surface and the droplet dries out, a ring of coffee or salt particles is left on the surface(Deegan, et al., 1997). This phenomenon exists not only in everyday life, but also in many practical industrial processes and scientific research and could also be used to assist in DNA sequence analysis, if the flow field in the droplet produced by the evaporation could be understood and predicted in detail.

In order to measure the fluid flow in a droplet, small particles can be suspended into the fluid as tracers. From the ratio of gravitational force to Brownian force $a^4 \Delta\rho g / k_B T$, we find that particle's tendency to settle is proportional to a^4(a is particle radius). So, to keep the particles from settling, the droplet size should be chosen to be in a range 0.1 -1.0μm in experiments. For such small particles, the Brownian force will affect the motion of the particle preventing accurate measurement of the flow field. This problem could be overcome by using larger particles as tracers to measure fluid flow under microgravity since the gravitational acceleration g is then very small. For larger particles, Brownian force would hardly affect the motion of the particles. Therefore, an accurate flow field could be determined from experiments in microgravity.

Deegan et al.(1997) measured the radial, height-averaged velocity distribution in an evaporating droplet and observed the formation of a ring. Their experimental results agreed well with the results of the theoretical analysis which they also carried out. Kantor(1997) also derived a velocity field using a different expression for the evaporation rate than that used by Deegan et al. Both expressions predict a height-averaged outward radial flow in an evaporating droplet. But both theories give only an expression for the radial height-averaged velocity.

In this paper, we will investigate the fluid flow in an evaporating droplet under normal gravity, and compare experiments to theories. Then, we will present our ideas about the experimental measurement of fluid flow in an evaporating droplet under microgravity.

THEORY

Let us consider a droplet on the surface, as shown in fig.1. The process of its evaporation is often divided into two phases. In the first phase, the contact angle decreases while the contact line holds its original position. In an evaporating droplet with a fixed, or pinned, contact line, the liquid must flow radially outward for the contact line to maintain its position, and the contact angle decreases with time as the droplet volume

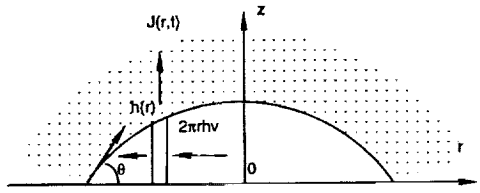

Fig. 1 A droplet on the surface

decreases. When the contact angle decreases to a critical angle, the second phase of evaporation starts. In this second phase, the contact line recedes while the contact angle remains constant(D. M. Anderson et al., 1995). The rate of decrease of the contact angle in the first phase depends on the evaporation rate of the droplet. Therefore, the evaporation of liquid induces the fluid flow in a droplet. From the theory of diffusion and a mass balance in the droplet, the relationship between the height-averaged velocity and local evaporation rate was obtained:

$$\rho\frac{\partial h}{\partial t} + \rho\frac{1}{r}\frac{\partial(rvh)}{\partial r} = -J(r,t) \qquad (1)$$

Here, the boundary condition is r=0, rvh=0. v is the height averaged velocity, $J(r,t)$ is the local evaporation rate. Deegan et al. and Kantor respectively developed their own expressions for the local evaporation rate. From the theory of Deegan et al., the local evaporation rate is:

$$J = J_o(1-r^2)^{-\lambda} \qquad (2)$$

where J_o is the evaporation rate when $\lambda = 0$, and λ controls the heterogeneity of droplet evaporation.

From the theory of Kantor, the local evaporation rate is:

$$(\hat{n} \bullet J) = \frac{A}{R}\left[2\arctan\left(e^{-\lambda'}\right)\sqrt{\sinh^2(\lambda') + \sin^2(\mu)}\right]^{-1} \qquad (3)$$

where $A = 17.28(1-H)\sqrt{T}\exp\left(\frac{-5283}{T}\right)$, H is the ambient humidity, $\delta \equiv \tan\left(\frac{\theta}{2}\right) \equiv \tanh(\lambda')$, θ is the contact angle, $\hat{n}$ is an outward-pointing normal vector at some point on the oblate surface, and λ' and μ are the parameters of the oblate spheroid, defined such that at the surface of the droplet, the r and z coordinates satisfy:

$$\frac{r^2}{(\cosh\lambda\cos\mu)^2}+\frac{z^2}{(\sinh\lambda\sin\mu)^2}=1$$

Combining (1),(2) and (3), the radial height-averaged velocity v for different theories were derived. From the theory of Deegan et al., it is:

$$v=\frac{1}{4}\frac{R}{t_f}\left[\frac{M(0)}{M(t)}\right]\tilde{r}^{-1}\left(\left(1-\tilde{r}^2\right)^{-\lambda}-\left(1-\tilde{r}^2\right)\right) \quad (4)$$

where $M(0), M(t)$ are the mass of the droplet at time 0 and time t, $\tilde{r}=r/R$ is the dimensionless radial position of a particle.

From the theory of Kantor, the radial height-averaged velocity is:

$$v=\frac{A\sqrt{1-\delta^2}}{2R\alpha\delta}\frac{1}{\tilde{r}(1-\tilde{r}^2)}\left[\frac{1+\delta^2}{1-\delta^2}\left(\sqrt{1-\tilde{r}^2(1-\delta^2)}-1\right)+\frac{1}{6\delta^4}\left(\frac{\left(\left(1-\delta^2\right)^2-2\delta^2\left(1-\tilde{r}^2\right)\right)\sqrt{\left(1+\delta^2\right)^2-4\delta^2\tilde{r}^2}-}{\left(1+\delta^2\right)\left(\left(1-\delta^2\right)^2-2\delta^2\right)}\right)\right] \quad (5)$$

where $\alpha=\arctan\left(\sqrt{\frac{1-\delta}{1+\delta}}\right)$ and the variable δ is calculated by integrating the following equation:

$$\frac{\partial\theta}{\partial t}=-4\frac{A}{R^2}\left[\arctan\left(\sqrt{\frac{1-\delta}{1+\delta}}\right)\sqrt{1+\delta^2}\,(1+\delta^2)^2\right]^{-1}$$

$$\delta=\tan\left(\frac{\theta}{2}\right)$$

The local radial and vertical velocity v_r and v_z must satisfy the continuity equation:

$$\frac{\partial(rv_r)}{\partial r}+\frac{\partial(rv_z)}{\partial z}=0 \quad (6)$$

For the solvent with low surface tension, the droplet on the surface is flat, so the lubrication theory can be applied. This implies that the radial velocity profile is parabolic. We also take the shear stress at the droplet surface to be zero; hence $\frac{\partial v_r}{\partial z}=0$ at z=h(r). Thus,

$$v_r=A'(z-2h)z \quad (7)$$

The relation between v_r and v is therefore:

$$v_r=\frac{3}{2}v\left(\frac{2z}{h}-\frac{z^2}{h^2}\right) \quad (8)$$

Once the evaporation rate is specified, v_r and v_z are obtained by combining eqns.(4),(5),(6) and(8). From the theory of Deegan et al., they are:

$$v_r=\frac{3}{8}\frac{R}{t_f-t}\frac{1}{\tilde{r}}\left[\left(1-\tilde{r}^2\right)^{-\lambda}-\left(1-\tilde{r}^2\right)\right]\left[2\left(\frac{z}{h}\right)-\left(\frac{z}{h}\right)^2\right] \quad (9)$$

$$v_z=\frac{3}{8}\frac{R}{t_f-t}\frac{1}{\tilde{r}}\left[\lambda\left(1-\tilde{r}^2\right)^{-\lambda-1}+1\right]\left[3\left(\frac{z}{h}\right)^2-\left(\frac{z}{h}\right)^3\right] \quad (10)$$

Likewise, from Kantor's theory, the local radial and vertical velocity v_r and v_z are:

$$v_r=\frac{3A\sqrt{1-\delta^2}}{4R^2\alpha\delta}\frac{1}{\tilde{r}(1-\tilde{r}^2)}\left[\frac{1+\delta^2}{1-\delta^2}\left(\sqrt{1-\tilde{r}^2(1-\delta^2)}-1\right)+\frac{1}{6\delta^4}\left(\frac{\left(\left(1-\delta^2\right)^2-2\delta^2\left(1-\tilde{r}^2\right)\right)\sqrt{\left(1+\delta^2\right)^2-4\delta^2\tilde{r}^2}-}{\left(1+\delta^2\right)\left(\left(1-\delta^2\right)^2-2\delta^2\right)}\right)\right]\left(\frac{2z}{h}-\frac{z^2}{h^2}\right) \quad (11)$$

$$v_z=-\frac{3A\sqrt{1-\delta^2}}{4R^2\alpha\delta}\frac{1}{(1-\tilde{r}^2)^2}\left[\frac{1+\delta^2}{1-\delta^2}\left(\frac{2-\left(1-\delta^2\right)\left(1+\tilde{r}^2\right)}{\sqrt{1-\tilde{r}^2\left(1-\delta^2\right)}}-2\right)+\frac{1}{6\delta^4}\left(\frac{2\left(1-\delta^2\right)^2\sqrt{\left(1+\delta^2\right)^2-4\delta^2\tilde{r}^2}-}{\sqrt{\left(1+\delta^2\right)^2-4\delta^2\tilde{r}^2}}-\frac{4\delta^2\left(\left(1-\delta^2\right)^2-2\delta^2\left(1-\tilde{r}^2\right)\right)\left(1-\tilde{r}^2\right)}{2\left(1+\delta^2\right)\left(\left(1-\delta^2\right)^2-2\delta^2\right)}\right)\right]\left(\frac{z^2}{h}-\frac{z^3}{3h^2}\right) \quad (12)$$

EXPERIMENTS

To determine which of the above two theories more closely approximates the real behavior, we measure the velocity field in an evaporating droplet. In these experiments, fluorescent particles of diameter around 0.74μm are used as tracers to obtain the flow path lines in the droplet.

An inverted fluorescent microscope(Nikon eclipse TE 200, 40x Power objective)is used to observe particle motion in the droplet. Droplets of radius 800-1000μm are spotted onto a glass substrate using an Eppendorf pipette (adjustable volume:0.5-10μl).

In order to measure the velocity field in the droplet we constructed the simple apparatus shown in fig. 2. It is a small cell covered by a millipore membrane to slow down the evaporation rate and keep the droplet from being disturbed by air currents. The millioprc filters used contain 6×10^8 holes per cm^2 of diameter=0.15μm. Using these filters, the droplet evaporation could be slowed down enough that the droplet evaporation time t_f could be made as long as 2 to 3 hours. Such long times are needed to allow time for measuring the initial droplet position and size and to track carefully a particle position as a function of time.

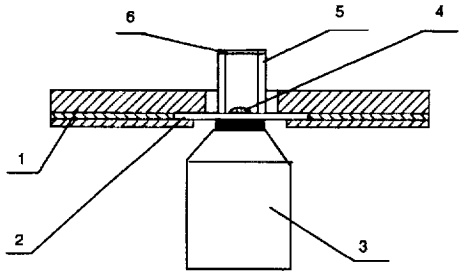

1. Support 2. Glass coverslip 3. Inverted microscope objective
4. Droplet 5. Seal Cylinder 6. Porous Membrane

Fig. 2 Experimental Apparatus

The suspension of fluorescent particles obtained from Polysciences was diluted 2000-fold to obtain a solution with a particle concentration of 125ppm. After spotting a droplet onto the coverslip and confining it in the geometry shown in fig. 2, we first measure the position of the contact line along the edge of the droplet. We then measure the air-water surface profile of the droplet at different times so that the volume vs. time can be determined. Finally, we choose a particle in the droplet and follow its motion with time, recording the particle's coordinates in the droplet at various times, yielding a three dimensional path line.

RESULTS AND ANALYSIS

1. The shape of droplet and droplet evaporation rate

Since the rate of decrease in droplet volume with time is a key parameter in the droplet evaporation models, a series of droplet profiles are measured at different times. In fig. 3, the symbols are the measured droplet surface profiles determined form the maximum vertical heights at which particles could be found at each radial position r at time t. Data could not be obtained near the center of the droplet because of the limited working distance of the objective, which did not permit viewing of the very top of the droplet. Nevertheless, enough of the profile is obtained to permit a fit by the profile expected for the droplet, namely that of a spherical cap.

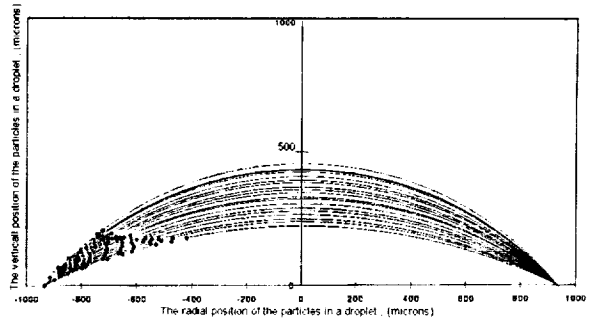

Fig. 3 The surface profiles of the droplet at different times

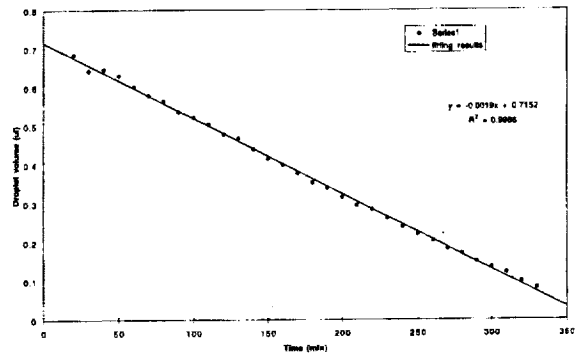

Fig. 4 The droplet volume as a function of time

The droplet volume at each time is calculated using the spherical-cap model and plotted in fig. 4. The volume of the droplet decreases linearly with time. This implies that the overall evaporation rate of the droplet is almost constant, which agrees with the theory of Deegan, et al. and the experimental results of Rowan, et al.(1995). From theory of Deegan et al., the overall evaporation rate $\dot{m}$ is:

$$\dot{m} = \frac{M(0) - M(t)}{t} = \frac{V(0) - V(t)}{t} \rho \quad (13)$$

where V(t) is the volume of the droplet at time t and ρ is the density of the solvent. So, from the experimental data of droplet volume vs. time, we can obtain the drying time, overall evaporation rate, and initial volume of the droplet by fitting experimental data with a straight line, as shown in fig.4(solid line).

The theory of Kantor predicts an overall evaporation rate that depends on contact angle as:

$$\frac{\partial V}{\partial t} = \frac{-\pi R A \sqrt{1-\delta^2}}{\alpha}, \delta \equiv \tan\left(\frac{\theta}{2}\right) \quad (14)$$

If the initial contact angle is small, eqn. (14) becomes:

$$\frac{\partial V}{\partial t} \approx -4RA\left[1 + \frac{2}{\pi}\delta + O(\delta^2)\right] \quad (15)$$

From eqn. (15), we can see that when the initial contact angle is small, Kantor's theory predicts that the overall evaporation rate will be almost constant.

2. Particle's path in the droplet.

Two typical experimental results are plotted in figs 5 and 6. The filled and open symbols are the experimental radial and vertical positions of a particle as a function of time. The radial position(open symbols) increases and the vertical position(filled symbols) decreases, showing that the particle moves toward the edge of droplet and toward the substrate as drying progresses.

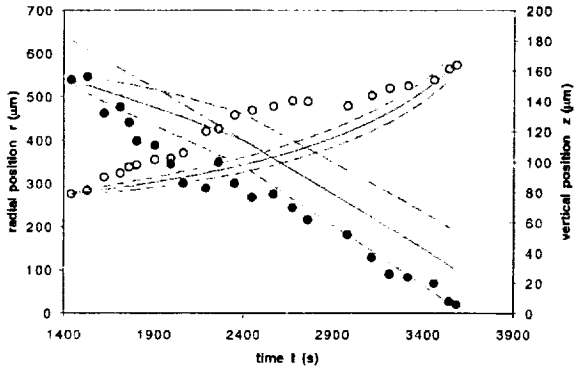

Fig. 5a The position of particle vs. time for λ=0.5 according to the theory of Deegan, et al.

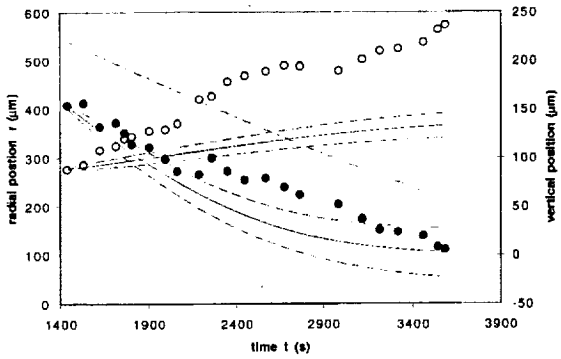

Fig. 5b The position of particle vs. time for H=0.975 according to the theory of Kantor

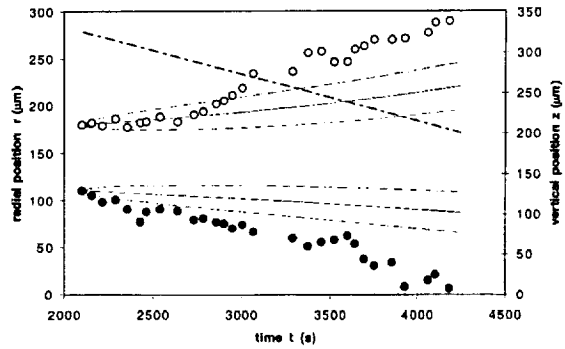

Fig. 6a The position of particle vs. time for λ=0.5 according to the theory of Deegan, et al.

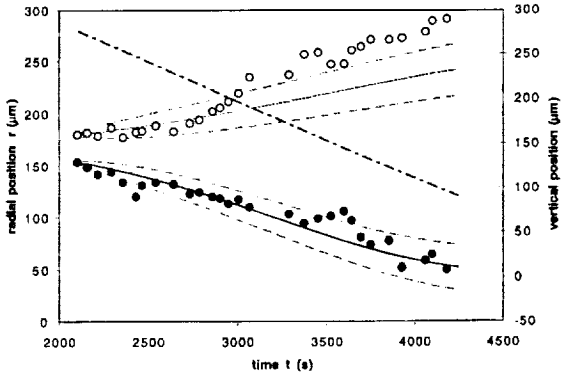

Fig. 6b The position of particle vs. time for H=0.975 according to the theory of Kantor

We also compare the experimental data with the theory of Deegan, et al. and of Kantor. Before we calculate the radial and vertical position of a particle in the droplet using the evaporation models, we must to find the parameter λ in the model of Deegan,et al. (equations 9 and 10) and the humidity H in the Kantor's model(equations 11 and 12). In order to find λ and H, we adjust λ and H so that the time for a particle in the center of the droplet, which is supposed to be fixed on the surface of the droplet, to reach the glass substrate is equal to the drying time of the droplet.

Using the fitted λ and H, we calculate the radial and vertical position of a particle in the droplet predicted by the two theories; these predictions are plotted in fig. 5 and 6. In each figure the solid line is that calculated from the theory without Brownian motion, while the dashed lines show the range of deviations expected to be produced by Brownian motion, using the theoretical diffusivity value. In general, the vertical position of the particle agrees with the prediction of both theories to within the experimental error due to Brownian motion. In one case(fig. 5), the predictions of the model of Deegan at al. are somewhat better than those of Kantor's model, while the reverse is true in fig. 6. The predictions of the radial velocity do not

agree as well with the experiments as do the predictions of the vertical velocity.

3. Additional predictions

3.1 The fluid velocity in the droplet.

From eqns. (9) to (12), we calculate the vertical and radial velocities respectively, which are plotted in figs 7 and 8 for the theory of Deegan et al. and Kantor at times 4400 sec. Here we have taken the droplet radius R to be 797μm, its height h(0) to be 365μm and the drying time t_f to be 4480 sec.. We can see the velocity fields for the two theories differ significantly. In the theory of Deegan, et al., the radial velocity is higher than in the theory of Kantor, especially near the edge of the droplet. Kantor's theory shows a higher vertical velocity than does the theory of Deegan et al., so that when the droplet is nearly dry the velocity vectors point almost completely downward; see fig. 8.

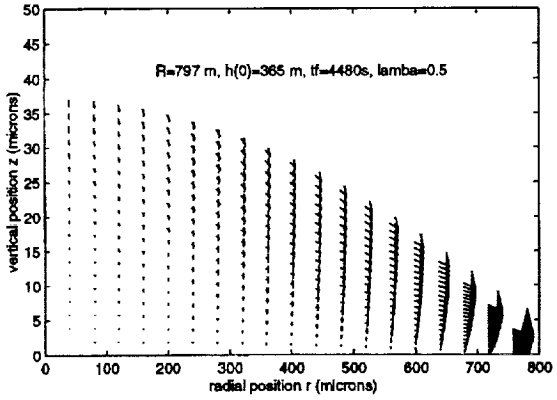

Fig. 7 The velocity field at t=4400s according to the theory of Deegan, et al.

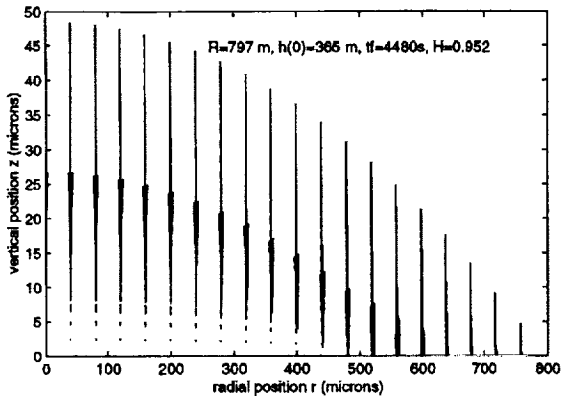

Fig. 8 The velocity field at t=4400s according to the theory of Kantor

3.2 Different evaporation conditions

By changing λ in the theory of Deegan, et al. and changing the H humidity in Kantor's theory, we can determine how the evaporation rate affects the calculated results. The results are plotted in figs. 9 to 12. In figs 9 and 10, we can see that the variation in r and z becomes larger with increasing λ. This implies that the more nonuniform the evaporation rate is, the stronger the flow is. In figs. 11 and 12, a decrease in the humidity produces an increase in the driving force for mass transfer during evaporation, and so the variations in z and r also become larger.

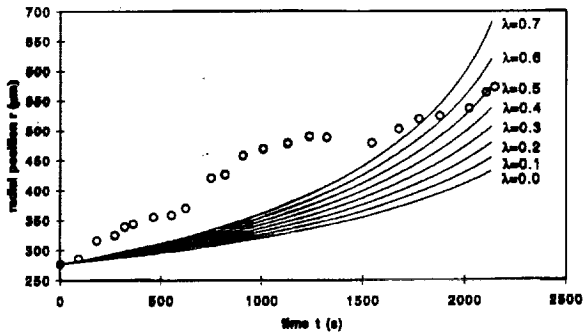

Fig. 9 The effect of λ on the time-dependent radial position of a particle

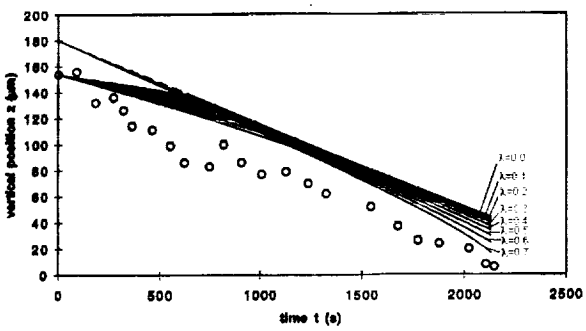

Fig. 10 The effect of λ on the time-dependent vertical(solid lines) position of a particle and the local height(dashed lines) of the droplet

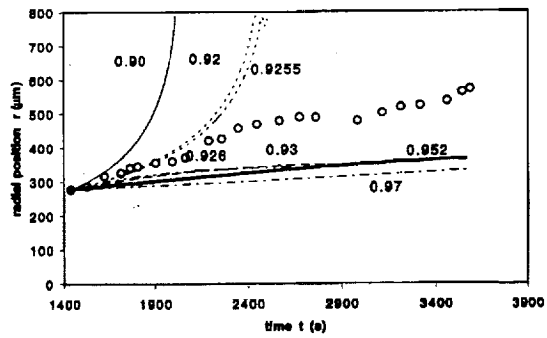

Fig. 11 The effect of humidity H on the time-dependent radial position of a particle from Kantor's theory

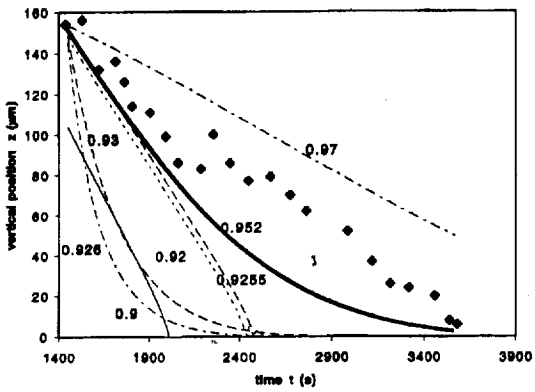

Fig. 12 The effect of humidity H on the time-dependent vertical position of a particle from Kantor's theory

CONCLUSION

1. Experimentally, the overall evaporation rate of an evaporating droplet is almost constant. This result agrees perfectly with the theory of Deegan, et al., and approximately with Kantor's theory.
2. The surface shape of droplet is that of a spherical cap.
3. The theory of Deegan et al. and that of Kantor give predictions of radial and vertical velocity that are in reasonable agreement with measured velocities, especially for the vertical velocity. A precise comparison is not yet possible, because of experimental error due to Brownian motion.
4. Near the end of the drying process, the theory of Deegan et al. predicts a much higher radial velocity than vertical velocity. For Kantor's theory, the vertical velocity is larger than the radial velocity near the end of drying.

ACKNOWLEDGE

We appreciate that NASA funds this project.

REFERENCE

1. D. M. Anderson and S. H. Davis, Phys. Fluids, 2:248(1995).

2. R. D. Deegan, O. Bakajin, T. F. Dupont, G. Huber, S. R. Nagel, T. A. Witten, Contact line deposits in an evaporation drop(to be published, 1996).

3. R. Kantor, A model of DNA Stretching in spots,(to be published, 1997).

4. S. M. Rowan, M. I. Newton, and G. McHale, J. Phys. Chem., 99:13268-13271(1995).